Published in Journal of Hydrology, Vol. 519, 2014, p. 2258–2271
which should be used for any reference to this work

Using tree ring data as a proxy for transpiration to reduce predictive uncertainty of a model simulating groundwater–surface water–vegetation interactions

O.S. Schilling [a,*], J. Doherty [c], W. Kinzelbach [b], H. Wang [d], P.N. Yang [e], P. Brunner [a]

[a] Centre for Hydrogeology and Geothermics (CHYN), University of Neuchatel (UniNe), Rue Emile-Argand 11, CH-2000 Neuchatel, Switzerland
[b] Institute of Environmental Engineering (IfU), Swiss Federal Institute of Technology Zurich (ETHZ), Wolfgang-Pauli-Str. 15, CH-8093 Zurich, Switzerland
[c] National Centre for Groundwater Research and Training (NCGRT), Flinders University, GPO Box 2100, Adelaide, SA 5001, Australia
[d] Hydrosolutions GmbH, Technoparkstr. 1, CH-8005 Zurich, Switzerland
[e] College of Hydraulic and Civil Engineering, Xinjiang Agricultural University, Urumqi 830052, China

S U M M A R Y

The interactions between surface water, the vadose zone, groundwater, and vegetation are governed by complex feedback mechanisms. Numerical models simulating these interactions are essential in quantifying these processes. However, the notorious lack of field observations results in highly uncertain parameterizations. We suggest a new type of observation data to be included in the calibration data set for hydrological models simulating interactions with vegetation: Tree rings as a proxy for transpiration. We use the lower Tarim River as an example site for our approach. In order to forestall the loss of riparian ecosystems from reduced flow over a 300 km reach of the lower Tarim River, the Chinese government initiated periodical, ecological water releases. The water exchange processes in this region were simulated for a cross-section on the lower reaches of the Tarim River using a numerical model (HydroGeoSphere) calibrated against observations of water tables, as well as transpiration estimated from tree ring growth. A predictive uncertainty analysis quantifying the worth of different components of the observation dataset in reducing the uncertainty of model predictions was carried out. The flow of information from elements of the calibration dataset to the different parameters employed by the model was also evaluated. The flow of information and the uncertainty analysis demonstrate that tree ring records can significantly improve confidence in modeling ecosystem dynamics, even if these transpiration estimates are uncertain. To use the full potential of the historical information encapsulated in the Tarim River tree rings, however, the relationship between tree ring growth and transpiration rates has to be studied further.

Keywords:
Model predictive uncertainty
Ecohydrology
Surface water groundwater interaction
Vadose zone
Tree ring growth
Transpiration

1. Introduction

The Tarim River in Xinjiang in northwest China (Fig. 1) is the most important source of water in the Tarim Basin (Cui and Shao, 2005). Over the last few decades, the rapid development of irrigation in the Tarim Basin has led to an increased demand for water. This threatens the riparian *Populus euphratica* forests in the lower reaches of the river, where water stopped flowing after the construction of Daxihaizi Reservoir (Fig. 1) in 1972 (Hou et al., 2007). In response to the severe degradation of these unique ecosystems, the Chinese government initiated the *Ecological Water Conveyance Project* (EWCP) in 2000. Its purpose is to conserve and restore the riparian ecosystems, and to prevent further desertification (Xu et al., 2007). These goals are to be achieved by periodically providing water from both Daxihaizi Reservoir and Lake Bostan (situated northwest of Daxihaizi Reservoir, Fig. 1) for flow downstream. Between 2000 and 2007, 11 ecological water releases were realized. These releases led to a rise of the water table in the vicinity of the river, and had a positive impact on the riparian vegetation (Chen et al., 2008): The tree ring growth record of *P. euphratica* indicates significant growth periods in response to the flow releases, as opposed to the pre-release tree ring record (Yang and Li, 2011; Yu et al., 2011).

Unfortunately, these ecological water releases come at high economic cost, as the water made available for the lower Tarim

* Corresponding author at: Centre for Hydrogeology and Geothermics (CHYN), University of Neuchâtel (UniNe), Rue Emile-Argand 11, CH-2000 Neuchâtel, Switzerland.
E-mail address: oliver.schilling@unine.ch (O.S. Schilling).

River could otherwise be used to support upstream agricultural production. In order to preserve the downstream ecosystems, while simultaneously minimizing the costs for the agriculture upstream, the flow releases have to be optimized. Optimal in this context means that only the amount of water required by the plants is made available to them; water that is not used by plants replenishes the vast regional groundwater systems and has minimal economical value. Understanding and quantifying the dynamics between infiltration along the river and transpiration of water through the riparian trees is therefore essential for an efficient allocation of the scarce water resources. Previous modeling studies have focused on specific aspects of the system, e.g. Yang et al. (2004) modeled hydraulic heads as a function of the Tarim River stream flow using analytical approaches without considering vegetation processes. To quantify and optimize the riparian water use efficiency (defined herein as the ratio of transpiration to infiltration from the river) of past and future water releases, however, a numerical model simulating all relevant processes is required. Parameters that govern hydraulic and vegetation processes need to be calibrated based on measurements of the system state.

Unfortunately, as is the case for many remote field sites, apart from hydraulic head measurements and some isolated discharge measurements, no other hydraulic data are available for the 321 km length of the lower Tarim River. This is problematic, as observations of hydraulic heads cannot fully inform parameters governing plant water uptake processes (Brunner et al., 2012). Given the limited availability and diversity of observations, the assessment of the overall efficiency of past and future ecological water releases is highly uncertain.

As indicated above, however, the previous flow releases have left a very clear signature in the tree ring growth record of the riparian vegetation (Yu et al., 2011). If it were possible to integrate the historic information encapsulated in the tree ring growth record, the calibration dataset could be significantly expanded, and the uncertainty of predictions of the riparian water use efficiency potentially reduced. But before a significant amount of tree ring growth data is acquired through expensive and time-consuming field campaigns along the Tarim River, a range of important questions have to be addressed:

(1) How can the historic information encapsulated in tree rings be used in the calibration of models simulating surface water, groundwater, and vegetation interactions?
(2) What is the data worth of tree rings? In other words, to what extent can tree ring growth data reduce the uncertainty of the predicted riparian water use efficiency beyond that afforded by observations of hydraulic heads?
(3) Which specific model parameters can be estimated with the new type of data?

This paper aims at answering these three questions, using the Tarim River site as an example. For this purpose, a numerical model that simulates the infiltration along the river, the flow through the unsaturated and saturated zones, as well as plant water uptake equivalent to transpiration is set up. The model is calibrated using hydraulic head observations, as well as transpiration estimates calculated from tree ring data. The worth of the different types of observation data in reducing the uncertainty of predicted infiltration and transpiration rates is quantified under consideration of their measurement uncertainty. Finally, an analysis on the flow of information from the calibration dataset to the calibrated parameters is carried out, providing fundamental insights into how the specific observations inform model parameters.

The results of this study are critical for modeling, data usage, and for the planning of future data acquisition and water release strategies in the Tarim Basin. Additionally, this work has significant repercussions to the rapidly growing field of modeling the interactions and feedback mechanisms between hydrological and ecological systems. To the best of the authors' knowledge this is the first study that integrates tree ring data (as a proxy for transpiration)

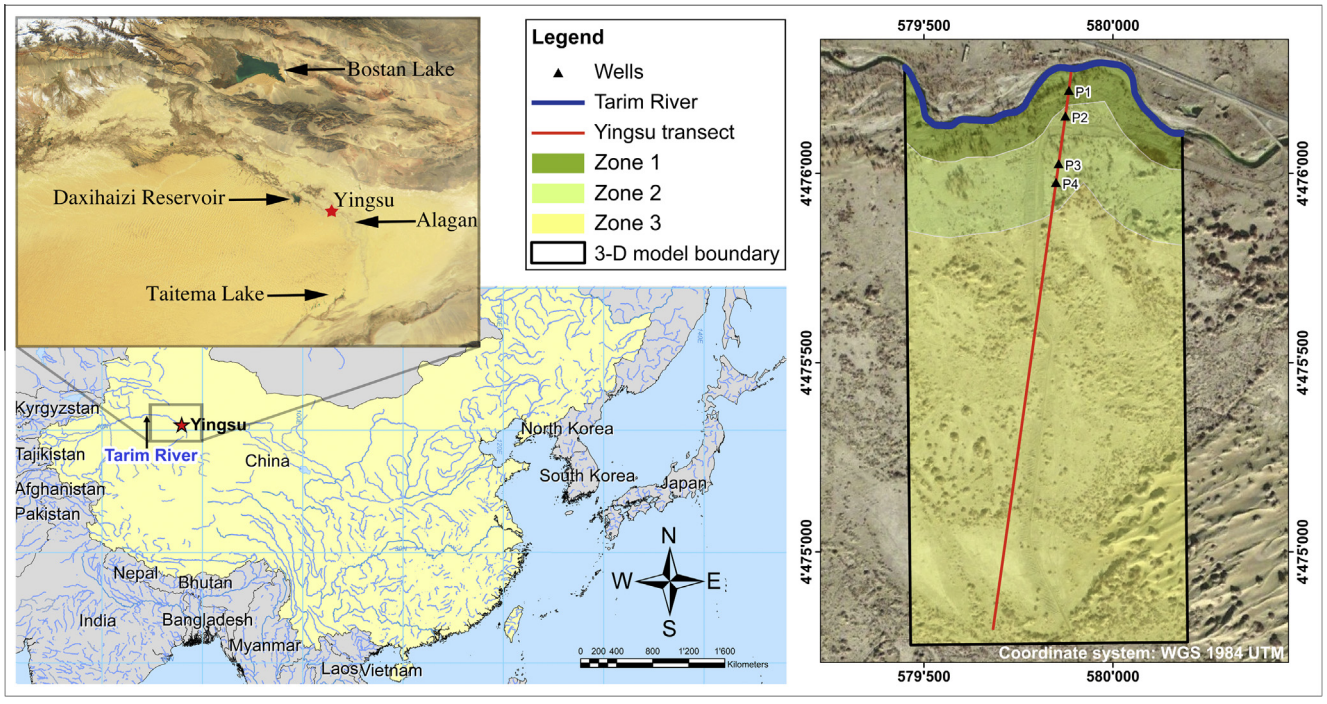

Fig. 1. The Yingsu study site on the lower Tarim River. The model outline, as well as the transect of observation wells (P1–4), and the three distinct zones of vegetation density are outlined in the satellite photo on the right hand side (available through GoogleEarth (2003)). The satellite image on the top left shows the middle and lower reaches of the Tarim River, Daxihaizi Reservoir, the Yingsu measurement site, as well as the three other important sites Alagan, Taitema Lake, and Bostan Lake, in the Tarim Basin (available through NASA (2001)). The location of the Tarim River in China is shown on the map on the bottom left corner.

into the calibration of a hydrological model and, for the first time, it is shown how such data can inform critical model parameters.

The paper is organized as follows: First the study site and the available data are described. Then the approach of estimating transpiration from tree ring growth for the use in the calibration process is explained. Descriptions of the conceptual and numerical model, as well as of the model calibration and validation, follow. Subsequently, the methods applied to quantify data worth, predictive uncertainty reduction, and flow of information, are described. Simulation results, together with data worth and the flow of information analyses are then presented. Discussion and conclusions complete this study.

2. Materials and methods

2.1. Study site

In order to document the response of the water table during the ecological water releases, the local authorities installed observation wells at 9 cross-sections along the lower Tarim River (Chen et al., 2009). For the subsequent analyses, data from the cross-section in Yingsu, located 61 km downstream of Daxihaizi Reservoir (Fig. 1) are used. This location was chosen due to the availability of local data of the channel geometry, the water level in the Tarim River during the releases, and the subsequent response in groundwater and tree ring growth. Climatic data are also available.

The channel section in Yingsu has a symmetric, trapezoidal shape, with a 10 m wide bed, a depth of 1.77 m and a bank slope of 2.2. The bed has an elevation of 832.4 m above sea level (ASL) and the bank of 834.11 m ASL The river flows over bare sand; no streambed or clogging layer has developed in the channel. The aquifer in Yingsu is unconfined, more than 40 meters deep and composed of homogeneous windblown sand (Hou et al., 2007; Yang et al., 2004). In total, 11 ecological water releases took place, but the first release was not properly documented in Yingsu, and after the 6th release water was routed through a new channel in the proximity of Yingsu. Therefore, only data of the first 5 documented releases are used in this study. These releases were named 2nd, 3rd(I), 3rd(II), 4th, and 5th(I). For better comprehension, the first documented release is hereby defined in this study as release 1 and incrementing numbers are assigned to the subsequent releases.

Discharge of releases 1–4 was measured at three measurement stations (Hou et al., 2007): at Daxihaizi Reservoir (0 km), in Yingsu (61 km) and in Alagan (143 km) (Fig. 1). The average infiltration between the stations was estimated by calculating the reduction of flow between Yingsu and the other stations (Table 1). With such limited data, however, a reliable estimation of the infiltration is not possible for a particular location.

In Yingsu, the response of the groundwater table to the ecological water releases was measured in 8 observation wells along a transect. However, only for four wells reliable and complete data are available. These wells were labeled C3, C4, C5 and C1; for ease of reading they are here referred to as wells P1, P2, P3, and P4, respectively, and are located at distances of 60 m, 130 m, 200 m, and 230 m perpendicular to the channel. The locations of P1–4 are shown in Fig. 1. Well P4 lies on the north side of the channel. Assuming that the flow of water at the transect is approximately symmetric and that the subsurface is homogeneous, in this study well P4 was mirrored onto the south side of the Yingsu channel (this assumption is validated in Section 2.3.5.). Measurements of the depth to groundwater are available from the beginning of release 1. The measured hydraulic heads in wells P1–4 during the extended 993-days period of the ecological water releases 1–5 as well as the surface water table in the Tarim River are illustrated in Fig. 2. From the available 96 groundwater level observations, 5 were removed from the subsequent analysis (as indicated in Fig. 2). These observations were obvious outliers that could only be explained by measurement errors.

Potential evapotranspiration (E_P) in the Tarim Basin amounts to 2750 mm per year. Annual rainfall is less than 50 mm, and due to the high E_P a negligible source of groundwater recharge for the region. Apart from water availability and E_P, the density of the vegetation cover controls transpiration. The vegetation cover is expressed by the dimensionless leaf area index (*LAI*). Ma et al. (2009) found an average *LAI* of 1.85 for individual *P. euphratica* trees. The density of *P. euphratica* trees decreases with increasing distance to the channel. An analysis of satellite images (GoogleEarth, 2003) allowed identifying three distinct zones of vegetation densities in Yingsu (indicated in Fig. 1). The trees were counted in a corridor of 100 m width along the transect. The highest density of *P. euphratica* is found up to 100 m distance from the channel (Zone 1, 0.007 trees/m^2), at a distance between 100 and 300 m from the channel the density is less (Zone 2, 0.003 trees/m^2), and at a distance between 300 and 1500 m, the density is very small (Zone 3, 0.00057 trees/m^2).

Yu et al. (2011) who studied tree ring growth in Yingsu subdivided the growth of *P. euphratica* into two periods, a low growth period prior to 2001 and a high growth period post 2001, indicating that water is the limiting factor for growth. Tree ring growth of the *P. euphratica* trees has been recorded along the transect in Yingsu since 1995 (Yang and Li (2011), pers. communication). The tree ring growth data available to this study (Table 2) were measured in 5 plots at different distances to the channel and measurements were taken on branches of similar circumference. A comparison of tree ring growth prior to 2000 to growth in 2003 reveals an increase of growth by up to a factor of 5.

In order to quantify the water balance for this system, and to understand the uptake of water through vegetation in response to the flow releases, information about transpiration is required. As transpiration was not measured in Yingsu during the water releases an approach to relate tree ring growth to transpiration has to be established.

Table 1
An overview over the duration of stream-flow in Yingsu as well as estimated infiltration volumes. Infiltration volumes were calculated using the discharge volumes from Hou et al. (2007). No information is available on release 5. The infiltration was separately calculated for the section between Daxihaizi Reservoir and Yingsu (Upstream) as well as for the section between Yingsu and Alagan (Downstream).

	Dates	Duration (days)	Infiltration (m^3/m per riverside)	
			Upstream	Downstream
Release 1	17.11.2000–07.02.2001	83	106	542
Release 2	04.04.2001–07.07.2001	95	82	152
Release 3	15.09.2001–19.11.2001	66	62	144
Release 4	24.07.2002–19.11.2002	119	88	136
Release 5	06.03.2003–29.04.2003	55	–	–
Total		418	338	974

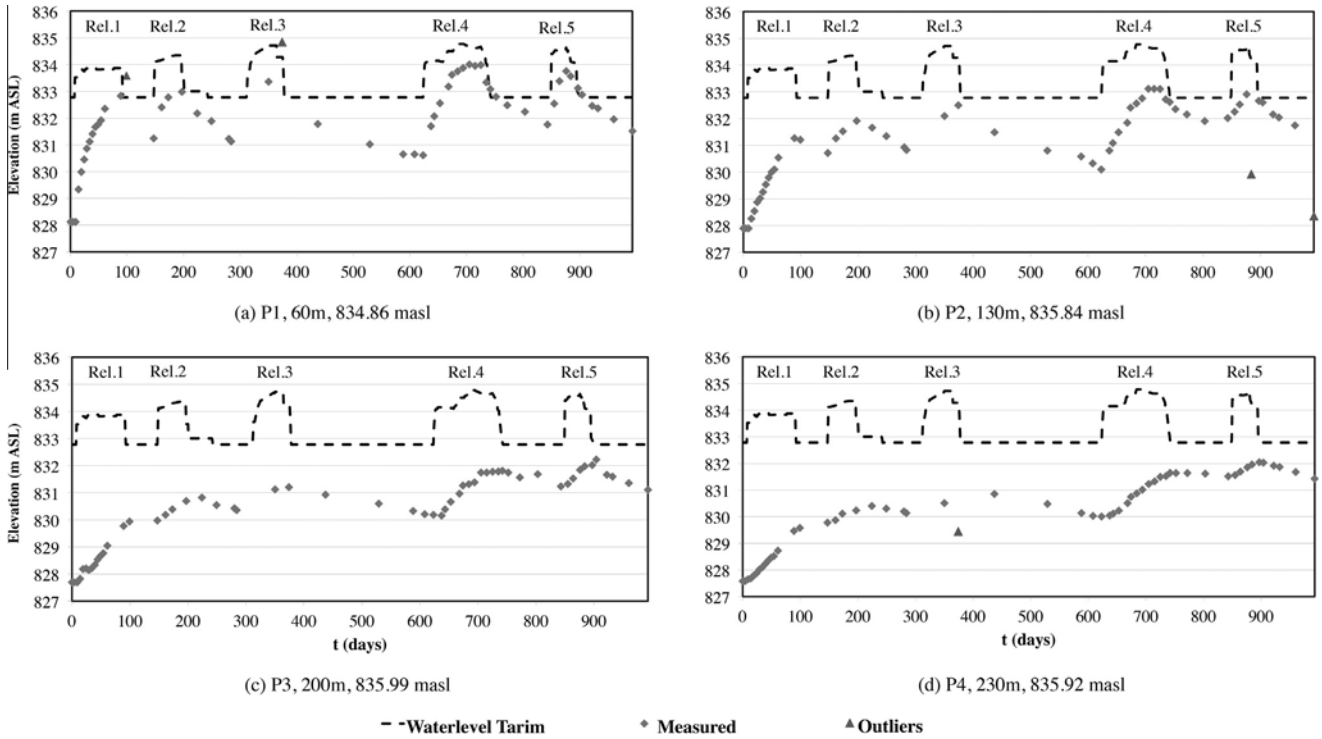

Fig. 2. The diamond markers represent the GW level measurements available for the period of 07.11.2000–28.07.2003, comprising releases 1–5, in wells P1–4. The dotted black line represents the surface water level in the Tarim River. Triangular markers indicate the four measurements that were removed from the analysis. Note that there is an extensive unsaturated zone with a thickness between 4 and 7 m; the thickness increases with increasing distance to the channel.

Table 2
Annual tree ring growth of *Populus euphratica* measured in Yingsu at different distances from the Tarim River. This data has been obtained through personal communication with Yang and Li (2011).

Distance to the river (m)	Annual tree ring growth (mm)					
	2000	2001	2002	2003	2004	2005
50	1.411	2.812	3.151	3.425		
150	1.907	2.106	2.371	2.552	2.620	2.296
350	1.191	2.306	2.268	2.288		
550	0.853	1.064	1.532	1.850		
1000	0.812	1.070	1.175	1.306		

2.2. Estimating transpiration from tree ring growth

Literature on transpiration rates of *P. euphratica* is scarce. Only three studies report transpiration of *P. euphratica* for the larger Xinjiang region (Chen et al., 2011; Fu et al., 2011; Si et al., 2007). For a number of reasons the application of these results to Yingsu is not straightforward. Chen et al. (2011) reported transpiration rates that exceed the E_P for Yingsu, and the data could therefore not be applied to this study. In the study of Fu et al. (2011) transpiration rates were reported in the form of standardized impact factors without further specifications. As insufficient information was provided to reconstruct the actual transpiration rates, the results of Fu et al. (2011) could not be integrated here. On the other hand, the study of Si et al. (2007) on *P. euphratica* proved to be crucial to this study. That study was carried out in the Ejina Basin, a neighboring basin with nearly identical environmental conditions as in Yingsu. In their detailed literature review, the authors demonstrate that their measurements of transpiration are plausible for the given climatic conditions, and in line with transpiration estimates of other species in similar environments. Si et al. (2007) measured transpiration of *P. euphratica* together with depth to groundwater; tree ring growth was, however, not reported. The depth to groundwater was measured in Yingsu and in the Ejina Basin and it therefore forms the key link between transpiration rates and tree ring growth.

Due to the limited data availability and remote nature of the field site a number of key assumptions had to be made to make use of the data provided by Si et al. (2007):

- The relations between depth to groundwater, tree ring growth, and transpiration in the Ejina Basin are the same as in Yingsu.
- The relation between tree ring growth and transpiration is linear for *P. euphratica*; In the only relevant publication on this subject known to the authors, Breda and Granier (1996) also found a near linear relationship between transpiration and tree ring growth, in their case for *Quercus petrea*.
- That tree ring growth is zero if transpiration is zero. This assumption is plausible because biomass production is inevitably linked to photosynthesis, which requires a certain degree of transpiration.

Based on the above-mentioned assumptions, the relationship between tree ring growth and transpiration was established, following the approach described below and illustrated in Fig. 3:

- In Fig. 3a tree ring growth in Yingsu (Yang and Li, 2011) is plotted as a function of the depth to groundwater. The data show that an increasing depth to groundwater is associated with decreasing growth, and that this relation is approximately linear.
- The average depth to groundwater and the corresponding transpiration of Si et al. (2007) are 2.9 m and 4.05 m^3/a, respectively. The two circle markers on the x-axis of Fig. 3a and b indicate these two values.
- The linear relationship based on the data between depth to groundwater and tree ring growth in Yingsu was used to calculate a corresponding value of tree ring growth for the measurement of Si et al. (2007) (Point A, Fig. 3a).

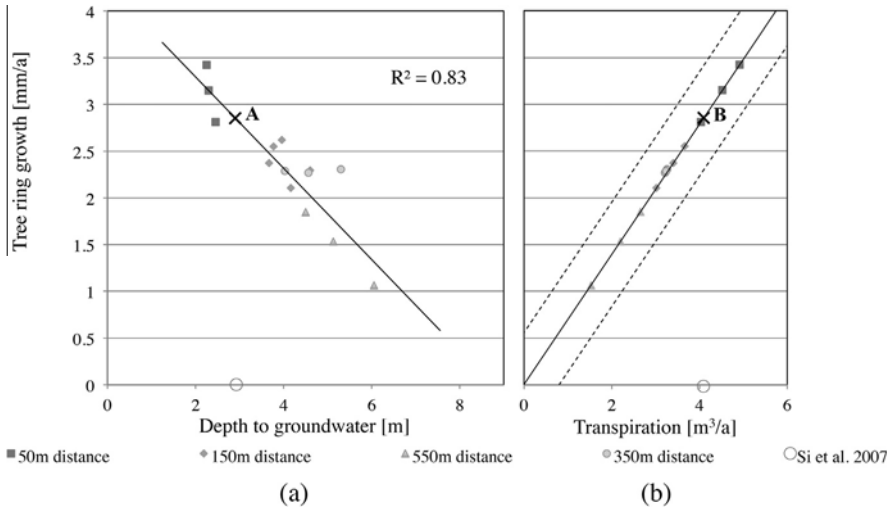

Fig. 3. (a) Tree ring growth of Populus euphratica as a function of the depth to groundwater in Yingsu (Yang and Li, 2011). The relation is approximately linear (Tree ring growth = −0.488 ∗ Depth to groundwater + 4.273). The different symbols correspond to different distances from the channel in Yingsu. (b) The estimated linear relationship between tree ring growth and transpiration (Tree ring growth = 1.434 ∗ Transpiration). The circles on the x-axes represent the depth to groundwater/transpiration measurement of Si et al. (2007). Point A and B represent the calculated tree ring growth for the value of Si et al. (2007). The transpiration uncertainty range of ±0.8 m^3/a is indicated in figure (b) by two dotted lines.

- This provides the first point for establishing the relation between transpiration rates and tree ring growth (Point B, Fig. 3b).
- The second point of the relationship between transpiration and tree ring growth is the coordinate origin (Fig. 3b).
- Under the plausible assumption that tree ring growth is zero for zero transpiration, and following the findings of Breda and Granier (1996) that the relation between tree ring growth and transpiration is linear, a linear relation defined through the coordinate origin and point B was established (Fig. 3b). This resulting linear function was used to convert each annual tree ring growth observation in Yingsu to a corresponding transpiration rate.
- Clearly, these estimates of transpiration are highly uncertain. An error of ±20% for the linking point B in Fig. 3b is assumed. This provides a sufficiently large margin to consider measurement errors of Si et al. (2007) but also to account for uncertainty related to the assumption of linearity. The assumed error translates into ±0.8 m^3/a for point B. The dashed lines in Fig. 3b represent this uncertainty in the transpiration estimates. The uncertainty is subsequently considered both in the calibration process (see Section 2.3.4.) as well as in in the predictive uncertainty analysis (see Section 3.2.). For the predictive uncertainty analysis even larger uncertainties are explored.

The estimated annual transpiration rates were then multiplied by the number of trees found in the three vegetation zones (Fig. 1) that correspond to the distances of tree ring measurements. The resulting transpiration volumes are summarized in Table 3.

Table 3
Annual transpiration volumes for a cross-section of 1 m width in m^3. The total transpiration is the sum of the three different zones of vegetation.

	Annual transpiration volume per vegetation zone (m^3)			
	Zone 1	Zone 2	Zone 3	Total
2001	2.8	1.9	1.1	5.7
2002	3.2	2.0	1.5	6.7
2003	3.4	2.1	1.9	7.4

2.3. Modeling

2.3.1. Modeling strategy

A two-dimensional (2-D) cross-sectional model is used to simulate the dynamics along the Yingsu transect (the red line in Fig. 1). This modeling strategy was chosen because the computational demand for calibration and uncertainty analysis of a 2-D model is significantly smaller compared to a three-dimensional (3-D) model. Modeling Yingsu using a 2-D approach implicitly assumes that the meander does not have a significant three-dimensional influence on groundwater flow and the resulting riparian water use efficiency. The 2-D approach is validated, by comparing the 2-D to a 3-D model. The 3-D model simulates a bigger area surrounding the transect, as outlined in Fig. 1. The same parameter values are used in both models. The observations, the simulation results of the 2-D model, and the simulation results of the 3-D model are compared by looking at:

- Groundwater levels using absolute values.
- Groundwater levels using the root mean squared error (RMSE).
- Groundwater levels using the Nash Sutcliffe model efficiency (NSE) coefficient (Moriasi et al., 2007).
- Transpiration and infiltration.

After demonstrating that a 2-D model is a valid approximation for the flow field in Yingsu, the data worth of the observations in reducing the predictive uncertainty of the model is quantified. This allows calculating to what extent the historic information encapsulated in the tree rings complement observations of hydraulic heads. Finally, the flow of information from observations to calibrated model parameters is explored.

2.3.2. Modeling code

For a number of reasons, the fully-coupled, physically-based HydroGeoSphere (HGS) modeling code (Therrien et al., 2010) is used in this study. Above all HGS was chosen for its ability to simulate all the relevant processes simultaneously, which are: groundwater flow, infiltration, transpiration, evaporation, and the flow in the unsaturated zone. Neglecting the unsaturated zone under a river can lead to significant errors in simulating the dynamics between surface water and groundwater (Brunner et al., 2010),

especially in areas where substantial amounts of water can be stored in the unsaturated zone underneath the river bed, as is the case at the Tarim River site. Furthermore, *P. euphratica* extract water from both the saturated and unsaturated zones; HGS allows vegetation to extract water from both zones, and provides a detailed model output on both transpiration and evaporation separately. This is an essential advantage over other modeling codes, as the influence of vegetation on the water balance of the Tarim River region needs to be understood separate from normal soil evaporation.

The suitability of HGS in similar modeling contexts has been demonstrated in a number of studies, e.g. Doble et al. (2011) who simulated infitration in response to surface water waves, or Banks et al. (2011) who simulated the interaction between surface water and vegetation. Calibration and uncertainty analysis with PEST has been successfully used in conjunction with HGS (Brunner et al., 2012).

The governing equations of HGS are described in detail in the Appendix A. Subsurface flow in HGS is simulated based on the Richards equation. Saturation is related to the relative permeability (k_r) and to pressure using the approach of Van Genuchten (Therrien et al., 2010). The calculation of evapotranspiration is based on the approach presented by Kristensen and Jensen (1975) (as employed by Panday and Huyakorn (2004)). In the approach of Kristensen and Jensen (1975), plant transpiration is a mechanistic function of E_P and three scaling functions:

- The first relation describes the linear dependency of transpiration on the *LAI* and is parameterized using the two constants C_1 and C_2. Transpiration increases with increasing *LAI* (see f_1 in the Appendix A).
- The second relation describes the dependency of transpiration on the soil moisture content: the full transpiration potential is reached at a soil moisture content between the field capacity (θ_{fc}) and the oxic limit (θ_{ox}). Transpiration approaches zero above θ_{ox} and below the wilting point (θ_{wp}). This relation is parameterized using the constant C_3 (see f_2 in the Appendix A).
- The third relation describes the dependency of transpiration on the root depth (*rd*): The *rd* defines the maximum depth of transpiration, and the amount of water transpired per depth depends on the root mass distribution (see the root distribution function (RDF) in the Appendix A).

If E_P is not reached through transpiration alone water is removed by direct soil evaporation, which reduces with increasing depth and is limited by an extinction depth (*ET depth*). Below the *ET depth* water cannot be mobilized for direct soil evaporation on the surface; only roots can access deeper water for evapotranspiration.

2.3.3. Numerical model

2.3.3.1. Geometry. The transect is modeled in 2-D as an unconfined aquifer of 1500 m width and a minimum of 30 m saturated plus 5–9 m unsaturated thickness. The base elevation of the model is 797 m ASL. As the model is a 2-D cross-sectional model, the model thickness is one unit (1 m). The topography along the transect was surveyed at 7 points to a distance of 1500 m from the river (Yang et al., 2004). The topography of the cross-section was interpolated in a linear fashion from these known points of elevation. The Tarim River in Yingsu is approximately symmetric with respect to the flow direction, and therefore, only half space, i.e. the southern side of the river, is modeled to reduce the computational demand by a factor of two. The observation wells are simulated at the distance that corresponds to their perpendicular distance to the channel.

The 3D model only simulates the southern side of the Yingsu channel section as well. The same channel and aquifer geometries are used in both models. The total length of the channel in the 3-D model is approximately 1000 m and the floodplain area has an extent of approximately 1 million m^2. For the 3-D model the topography of the Yingsu region was obtained from a 90 m-resolution digital elevation model (DEM) from the Shuttle Radar Topographic Mission (SRTM) (Jarvis et al., 2008). The DEM was adjusted by −7 m in order to match the unknown reference system of Yang et al. (2004).

2.3.3.2. Temporal and spatial discretization. Horizontally, the 2-D cross-sectional model consists of a rectangular grid with 222 cells that become narrower the closer they lie to the Tarim River. In the channel the resolution is 0.15 m. The high resolution within the channel and its bank ensures that the relation between water depth and wetted perimeter is following the real bathymetry. Vertically, the model is divided into 120 layers. The vertical node spacing in the lower part of the model domain is 0.875 m. The unsaturated zone is discretized with a maximum vertical resolution of 0.175 m. The spatial discretization of the 2-D cross-sectional model is shown in Fig. 4.

The 3-D model is spatially discretized with a lower resolution using a triangular grid (in contrast to the 2-D model). This slightly different approach was chosen to better represent the outline of the channel. Horizontally, the resolution decreases stepwise at distances of 6 m, 60 m and 250 m from the centerline of the channel. In the vertical direction, the model is subdivided into 31 layers. The top four layers have an approximate height of 0.125 m, the following 23 layers of 0.5 m and the bottom 4 layers of 7 m each. The spatial discretization of the 3-D model is illustrated in Fig. 6.

An automatic time stepping scheme with a maximum time step size of 1 day and a minimum of 0.1 days is used for both models. The initial time step is 0.1 days.

2.3.3.3. Boundary and initial conditions. The base of the models, as well as the symmetry axis, which is represented by the centerline of the stream, is impervious. Groundwater flow along the river is assumed to be perpendicular to the stream and therefore the lateral boundaries of the 2-D and the 3-D models are also impervious. A steady water table 1500 m away from the channel has established during the decades without water flowing in the Tarim River. This is conceptualized through a constant head boundary condition with a hydraulic head of 827 m ASL. The stage in the Tarim River (represented by the dashed line in Fig. 2) is modeled as a time dependent head boundary condition based on the data presented in Fig. 2.

The initial groundwater table was obtained from the measured groundwater levels at the beginning of the first water release. No data were available for the depth to groundwater directly below the river and the water table was extrapolated from the

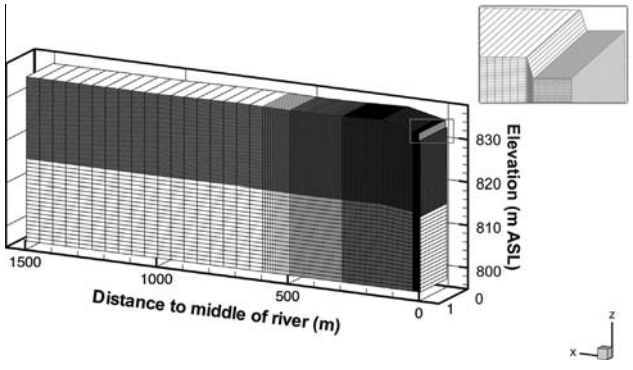

Fig. 4. Topography and spatial discretization of the Yingsu model. The closer to the channel in the top right corner, the finer becomes the mesh. The vertical coordinates have been exaggerated for better graphical presentation.

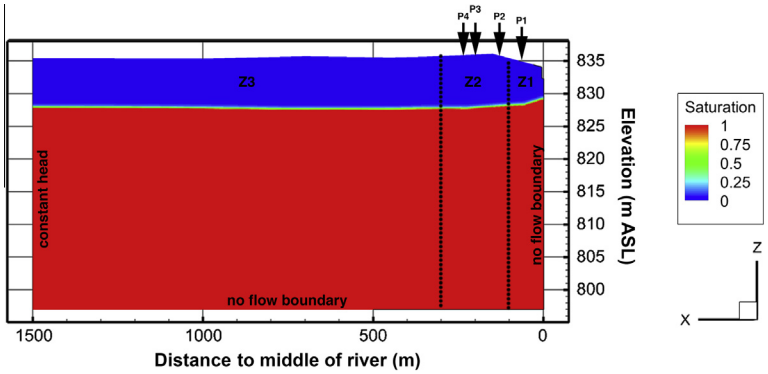

Fig. 5. The initial and boundary conditions of the 2-D model. The three zones of different vegetation densities (Z1, Z2, and Z3) are indicated by the dotted lines. The vertical coordinates have been exaggerated for better graphical presentation.

measurements at P2 and P1. Fig. 5 illustrates the initial water table of the 2-D model of Yingsu, the different boundary conditions, the locations of the observation wells, as well as the three different vegetation zones.

The initial water table of the 3-D model is shown in Fig. 6. The water table observed along the transect is assumed to be representative for the entire model area and used as initial condition for the entire 3-D model.

2.3.4. Model parameters and model calibration

The transient 2-D model was calibrated using the parameter estimation software PEST (Doherty, 2010a). PEST optimizes model parameters by minimizing a least squares objective function of differences between weighted observations and model outputs. A weight has to be assigned to every observation and is ideally representing the inverse of the measurement error. The 2-D model was calibrated against data from releases 1 and 2; the subsequent releases (releases 3–5, $t = 285$ until $t = 993$) were used for validation. The data of these 5 releases are considered representative of the rise and fall of the groundwater table and the reaction of vegetation in response the ecological water releases. The observation data sets used in the calibration were:

- Groundwater levels measured between 7. November 2000 ($t = 0$) and 19. August 2001 ($t = 285$), i.e. 23 observations for each of the four wells P1–4.
- A transpiration estimate representing the first 230 days of 2001, which are included in the calibration period (1. January 2001 ($t = 55$) –19. August 2001 ($t = 285$)).

A weight of 2, representing a very conservative measurement error of 0.5 m, was assigned to all groundwater level measurements. With a weight of 5 assigned to the transpiration estimate, visibility of transpiration in the calibration objective function was guaranteed; this being in accordance with the strategy recommended by Doherty and Welter (2010). The weight for transpiration was chosen in the following way: the inverse of the assumed measurement error of 0.8 m^3/a that was introduced in Section 2.2 is 1.25. Multiplying 1.25 by the number of observation wells (4) equals a weight of 5.

The calibrated parameters are shown in bold in Table 4. The upper and lower limits given to each parameter during calibration are shown in brackets. Uncalibrated parameter values were chosen for the following reasons: *LAI* values represent the reference *LAI* multiplied by the vegetation density per zone (see Section 2.1). The coupling length (l_{exch}) for the exchange between the river and the subsurface was set to a low value to reflect the fact that no clogging layer is present in the stream. By setting C_2 to 0

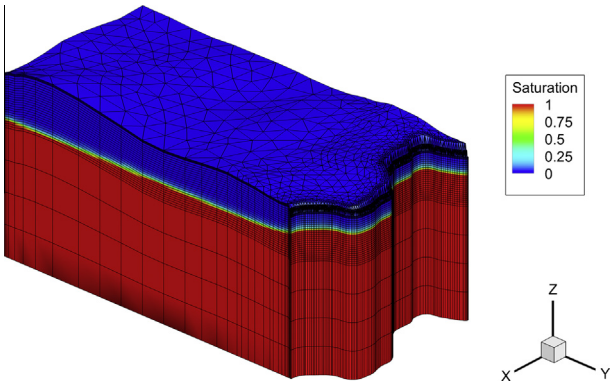

Fig. 6. Initial condition and topography of the 3-D model of Yingsu. The initial condition is the same as in the 2-D model. The smaller the distance to the channel, the higher becomes the resolution of the grid.

transpiration is inhibited when no trees are present (taking into account that no grass is growing there). C_3 was set to a high value to ensure rapid uptake of water by the trees, as these trees must be able to react immediately to the availability of water (see Appendix A for more details on C_2 and C_3). Trees that grow in arid environments, such as in the Tarim Basin, but that are periodically inundated, have developed root systems that allow taking up water even if their roots are fully submerged (Mitsch and Gosselink, 2007). This behavior is conceptualized by setting θ_{ox} to a relative saturation of 1.0 and the anoxic limit (θ_{an}) to 1.001. The choice of the ET depth is in line with studies on phreatic evaporation in

Table 4
List of model parameters. Parameters subjected to calibration and their optimized values are bold. For the calibrated parameters the lower and upper boundaries used in calibration are given in brackets. See the Appendix A for detailed descriptions of the parameters.

Aquifer parameters		Vegetation parameters	
K (m/d)	**1.84** (1–25)	C_1 (–)	**0.7** (0.01–200)
n (–)	**0.16** (0.1–0.42)	C_2 (–)	0
α (1/m)	**5.04** (4–14)	C_3 (–)	10
β (–)	**2.5** (1.01–2.9)	***rd*1** (zone 1) (m)	**3.5** (0.5–7)
S_{wr} (–)	0.02	***rd*2** (zone 2) (m)	**4.3** (1–9)
E_P (m/d)	0.0077	***rd*3** (zone 3) (m)	**6** (1–10)
ET depth (m)	0.5	*LAI*1 (zone 1) (–)	0.0777
l_{exch} (m)	0.001	*LAI*2 (zone 2) (–)	0.0333
		*LAI*3 (zone 3) (–)	0.006475
		θ_{wp} (–)	0.05
		θ_{fc} (–)	0.15
		θ_{ox} (–)	1
		θ_{an} (–)	1.001

similar regions of Xinjiang (Brunner et al., 2008; Hu et al., 2009; Li et al., 2009). Other parameters listed in Table 4 represent standard values for sandy soils.

2.3.5. 2-D model validation

2.3.5.1. Calibrated parameters. Calibrated parameter values are highlighted in Table 4. Values for the aquifer parameters hydraulic conductivity (K) and porosity (n) obtained in the calibration process compare well to the values found by Yang et al. (2004), and match the literature values for sandy soil types (Carsel and Parrish, 1988). The vegetation parameters are also reasonable: Root depths of the three distinguishable zones of vegetation density ($rd1$–$rd3$) are large enough to reach the saturated zone and match the depths that were found by Yang and Li (2011). No reported values of the fitting parameter C_1 for arid environments could be found in literature.

2.3.5.2. Comparison between the simulations and the measurements. In Fig. 7 the simulated and the observed groundwater levels are compared for the calibration and the validation period. For the 2-D model, the largest discrepancy exists for release 1 in observation well P1 (Fig. 7a). However, all of the following releases are reproduced with a significantly higher accuracy. The mismatch for release 1 therefore seems to be related to the missing information of the initial water table directly below the stream. The RMSE for the 2-D model are 0.39 m, 0.35 m, 0.32 m and 0.35 m for wells P1, P2, P3 and P4, respectively. The RMSE for all 4 observation wells together is 0.35 m. This mismatch lies within the estimated uncertainty range of groundwater measurements (0.5 m, see Section 2.3.4). Also the groundwater levels simulated with the 3-D model, which was not directly calibrated but based on parameter values obtained through calibration of the 2-D model, fit the measurements sufficiently well (total RSME of 0.69 m). As the simulations also match the data of the mirrored well P4 (see Section 2.1).

The simulated infiltration volume amounts to a total of 639 m^3/m per bank over all events. As discussed in Section 2.1, infiltration in Yingsu was not measured during the flood events, but average infiltration rates between Daxihaizi, Yingsu and Alagan could be estimated from discharge measurements (Table 1). The simulated infiltration rates correspond to the estimated average infiltration between the up- and downstream of Yingsu.

2.3.5.3. Comparison between the 2-D and the 3-D model. The 2-D model compares well to the 3-D model of the Yingsu area. A comparison of simulated groundwater levels is shown in Fig. 8a–d. Differences between the two models are more pronounced in the beginning of the simulation, possibly related to uncertainty in the initial groundwater levels. Considering the NSE coefficients for the groundwater levels of the two models, the models perform almost identically well, with a value of 0.97 for the 2-D and a value of 0.91 for the 3-D model (for the dimensionless NSE coefficient a value of 1 represents the best and a value of $-\infty$ the worst possible fit). Hence, the comparison of absolute groundwater levels, RMSE, and NSE reveal that 3-D effects are minimal and do not significantly affect the questions we seek to answer.

In addition to groundwater levels, the riparian water use efficiency was also compared between the models. The comparison revealed that the simulated efficiencies of the two approaches are nearly identical, providing further evidence that the 2-D approach is a valid approximation of the system. The efficiencies are further discussed in Section 3.1, and shown in Fig. 9.

2.3.6. Predictive uncertainty and data worth analysis

In order to assess the data worth of observations of hydraulic head and of estimates of transpiration, the pre- and post-calibration predictive uncertainties for a prediction of infiltration and for a prediction of transpiration are quantified using the PEST utility GENLINPRED (Christensen and Doherty, 2008; Doherty, 2010b). Linear uncertainty analysis can provide valuable insights into predictive uncertainty, even if applied to highly non-linear models (Brunner et al., 2012; Dausman et al., 2010). GENLINPRED establishes the worth of a particular observation by calculating how

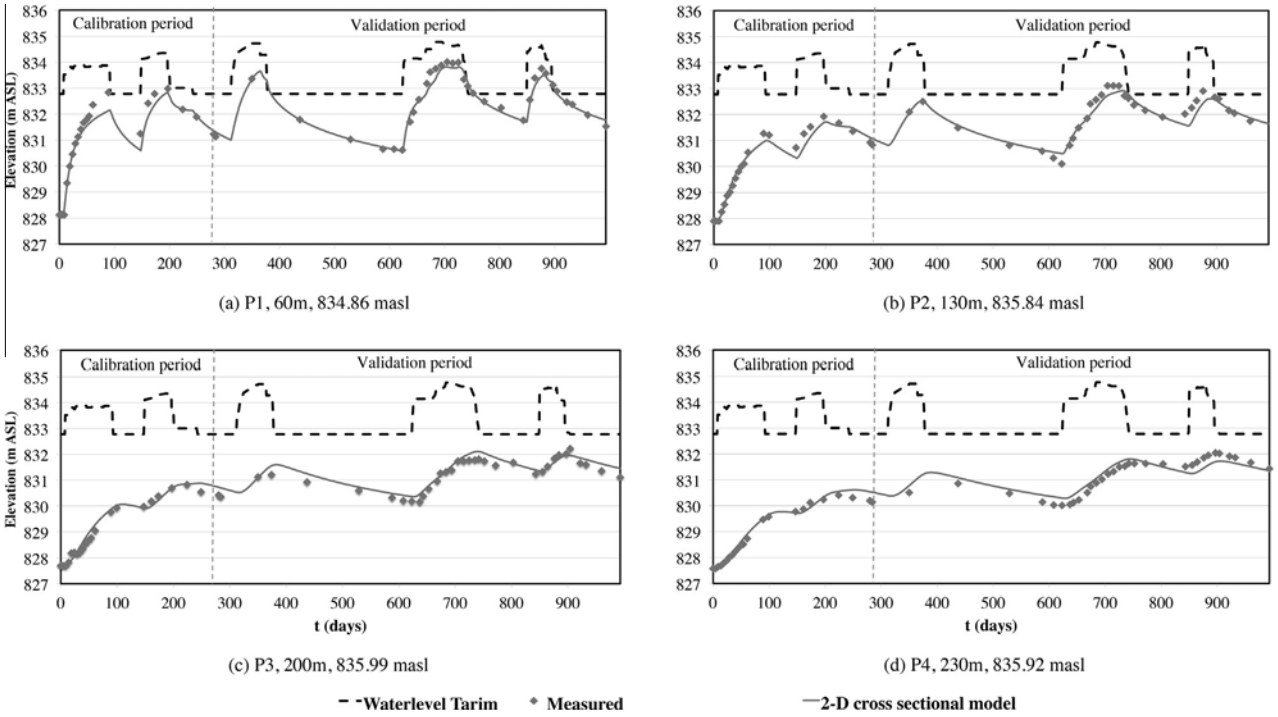

Fig. 7. Groundwater levels simulated with the calibrated 2-D model in comparison to the measured groundwater levels. Indicated is the calibration period (releases 1 and 2), as well as the validation period (releases 3–5).

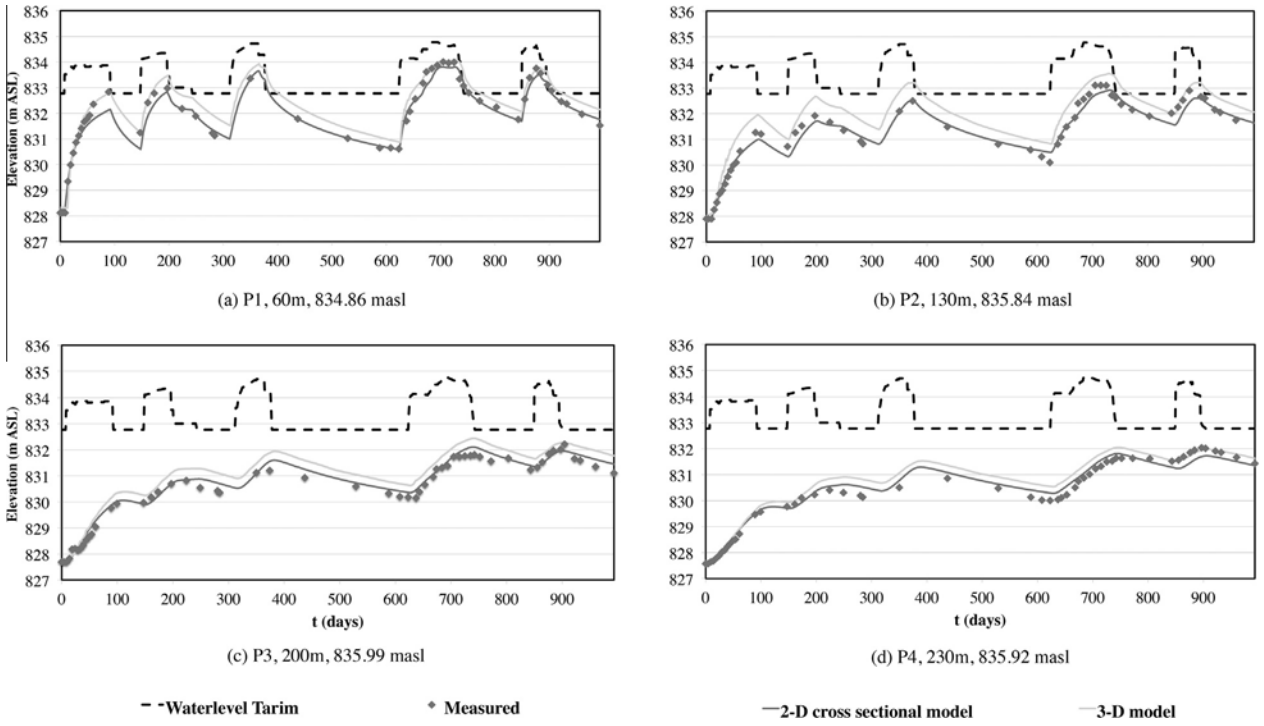

Fig. 8. Results of the simulations with the 3-D model, obtained with the parameters calibrated in the 2-D model. 3-D model results are compared to the measured groundwater levels and the 2-D simulation results.

much the uncertainty of a prediction can be reduced through inclusion of this individual observation in the calibration dataset. In this study the data worth of a whole group of elements of the calibration dataset is considered, i.e. either all hydraulic head observations together or the transpiration observations. The reduction in uncertainty of a prediction, achieved through inclusion of different observation groups in the calibration dataset, is a measure of data worth.

The influence of measurement uncertainty on predictive uncertainty can also be explored in this analysis by varying the weights given to the different observation groups during the calibration process. As mentioned above in Section 2.3.4 and described by Doherty and Welter (2010), the choice of weights can be a subjective process: While weights ideally represent the inverse of measurement uncertainty, both the number and distribution of measurement data points may require alternative weights in order to guarantee visibility of important measurements in the calibration objective function.

2.3.7. Flow of information analysis

While linear-type uncertainty analyses, as described above, are very useful to quantify the uncertainty of a given prediction, they do not provide insights into how exactly the observations used in the calibration process inform individual model parameters during calibration. This information can be extracted by the flow of information analysis: The flow of information from a calibration dataset to the parameters undergoing calibration can be tracked by subjecting the calibration sensitivity matrix to a Singular Value Decomposition (SVD) (Doherty, 2010a,b). Hill and Østerby (2003) showed that the SVD method performs equally well compared to other parameter correlation methods in identifying correlation between observations and parameters in groundwater flow models.

Quantifying the flow of information is mathematically more challenging than linear uncertainty analysis and requires a solid understanding of the concept of Eigenvectors and Singular Values. The detailed mathematics of this method and its application are described in the PEST manual (Doherty, 2010a,b) and in (Doherty and Hunt, 2009; Hill and Østerby, 2003). A qualitative description based on Aster et al. (2005) and Hill and Tiedemann (2007) is given here: Hill and Tiedemann (2007) describe that, in principle, applying SVD to the calibration sensitivity matrix yields the Eigenvalues, i.e. the Singular Values, and the associated Eigenvector pairs, i.e. the Eigenvector of parameters and the Eigenvector of observations. There are as many Eigenvector pairs coupled by Singular Values as there are parameters that are calibrated. Singular Values establish a ranking among the Eigenvectors. Eigenvectors that have Singular Values close to a maximum value of 1 indicate the highest flow of information, i.e. the most sensitive and informative couplings between observations and parameters. Analysis of the members of the Eigenvectors allows simultaneously identifying the sensitive parameters as well as the observations that inform these parameters. In each Eigenvector individual elements are associated with a coefficient between −1 and 1, and the squared sum of all coefficients amounts to 1. The coefficients are a measure of importance of an individual element relative to other elements of the same Eigenvector. Hence, in the Eigenvector of observations the magnitude of a coefficient is a measure of the ability to inform the paired Eigenvector of parameters. And vice versa, the magnitude of the coefficient of each parameter in the Eigenvector of parameters is a measure of its sensitivity to the paired Eigenvector of observations.

3. Results

3.1. Riparian water use efficiency

A volume of 18.3 m^3 of water is transpired during the 5 ecological water releases in the 2-D model ($t = 0$ until $t = 993$). This compares well with the volume estimated from tree ring growth (see Table 3). Regarding the riparian water use efficiency, the phreatophytes consume a total of only 2.9% of the water that infiltrates

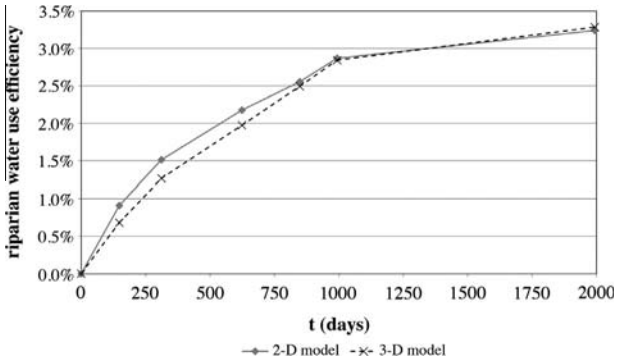

Fig. 9. Comparison of the riparian water use efficiency simulated with the 2-D and the 3-D models spanning the entire simulation period plus an additional 1000-days relaxation period without additional stream-flow.

during that time. The remaining 97.1% of the infiltrated water are stored in the aquifer. Part of this infiltrated water remains available to the trees. The ratio of simulated transpiration to infiltration increases with time: Simulation of 1000 additional days without further flooding after release 5 shows that the trees could potentially use up to a total of 3.24% of infiltrated water (Fig. 9). The riparian water use efficiency therefore improves over time. In order to complement the validation of the 2-D approach (see Section 2.3.5.), the efficiency calculated with the 3-D approach is also plotted in Fig. 9. The calculated efficiencies are essentially identical.

3.2. Predictive uncertainty and data worth

In order to analyze the data worth of the observation data, the data's potential to reduce the uncertainty for the prediction of the transpiration volume for 2002 (Table 3) and the infiltration volume for release 3 (Table 1) was quantified. The uncertainty of both predictions was calculated under consideration of the two groups of data used in calibration: i.e. observations of hydraulic heads (group H) and the estimate of transpiration (group T). The predictive uncertainty reduction was analyzed for the use of both groups of data separately (i.e. only H or T), as well as for their conjunctive use (H + T).

Recall that by systematically varying the weights associated to each observation group in the calibration dataset, the relation between measurement uncertainty and predictive uncertainty can be explored. The standard weights for this analysis are the weights used in the calibration process (see Section 2.3.4). The weights for H were kept constant, as the measurement accuracy is reasonably well known. As discussed in Section 2.2, however, the estimates of T are highly uncertain and the uncertainty might exceed the estimated 0.8 m^3/a. To explore this uncertainty, the weights for T were varied, ranging from the highest weight (5), as used during calibration, to a very small weight (0.01), representing a measurement uncertainty of 400 m^3.

The resulting predictive uncertainties, expressed as total uncertainty standard deviations, for the transpiration volume of 2002 and the infiltration volume of release 3 are listed in Table 5.

3.2.1. Prediction of the transpiration for 2002

If just an observation of T with a high weight of 5 is employed in the absence of observations of H, the predictive uncertainty of transpiration of 2002 can be reduced by a factor of 330 in comparison to the uncalibrated model. Even a very conservative weight of 0.05, representing a very high uncertainty for the observation of T, leads to a reduction of the predictive uncertainty of transpiration by a factor of 12.

When just observations of H are employed, a comparison of the pre-calibration with the post-calibration predictive uncertainty of transpiration reveals a reduction by a factor of 10; significantly less compared to using observations of T only.

The combination of both observation groups (H + T) is particularly helpful when the uncertainty of transpiration is very high, as could be the case for the estimates from tree ring growth. But if observations of T are more accurate (e.g. weights of 0.5 and 5), no further reduction of predictive uncertainty for predictions of transpiration can be achieved by complementing observations of T with observations of H.

3.2.2. Prediction of the infiltration for release 3

Surprising findings result for the prediction of infiltration. Employing the observation of T (weight 5), without observations of H, already reduces the predictive uncertainty of infiltration by a factor of 4.8; this is slightly above the reduction gained by employing observations of H only (a factor of 4.5). Even a very conservative weight of 0.01 for the observation of T yields a reduction of the predictive uncertainty of infiltration by a factor of 2.3. The combination of observations of H and T, with a high weight for T (5), results in the highest reduction, by a factor of 6.2.

This demonstrates that observations of T not only provide information about transpiration, but also about infiltration, as transpiration forms a key part of the water balance. They are especially valuable when their measurement accuracy is high.

3.3. Flow of information

The results of the SVD analysis, illustrated in Fig. 10, allow relating the information content of the observations to the parameters subject to calibration. The Eigenvector pairs are ordered by their importance in terms of flow of information, represented by the magnitude of their Singular Values. The pair with the highest Singular Value is shown in plots 10a&b, the second most important pair in plots 10c&d, and the third most important pair in plots 10e&f. Plots on the left hand side of Fig. 10a, c, and e represent the three Eigenvectors of observations. In each of these plots, the SVD coefficients of groundwater level observations are grouped by piezometer (P1–4, color coded) and plotted on the horizontal axis from left to right in order of time. As additional guidance the four solid lines associated with the secondary vertical axis indicate the measured groundwater levels over time for each piezometer separately. The single observation of transpiration (T) forms the last element on the horizontal axis of these plots. Plots on the right hand side of Fig. 10b, d, and f contain the three Eigenvectors of parameters, which are paired with the Eigenvectors of observations on the same row.

Table 5
The predictive uncertainty reduction for the transpiration of 2002 and the infiltration of release 3. H stands for calibration with hydraulic head measurements only, T for calibration with transpiration only, and H + T for combined calibration. Weights associated to individual observations within each observation group are indicated in brackets. The 2-D model was calibrated with H(2) + T(5).

	Predictive uncertainty									
	Pre-	Post-calibration total uncertainty standard deviation (m^3)								
	–	H(2)	T(0.01)	T(0.05)	T(0.5)	T(5)	H(2) + T(0.01)	H(2) + T(0.05)	H(2) + T(0.5)	H(2) + T(5)
Transpiration of 2002	427.8	43.2	161.2	34.7	3.7	1.3	41.9	27.2	3.7	1.2
Infiltration of release 3	211.2	46.8	89.2	46.7	43.6	43.6	46.2	39.7	34.3	34.2

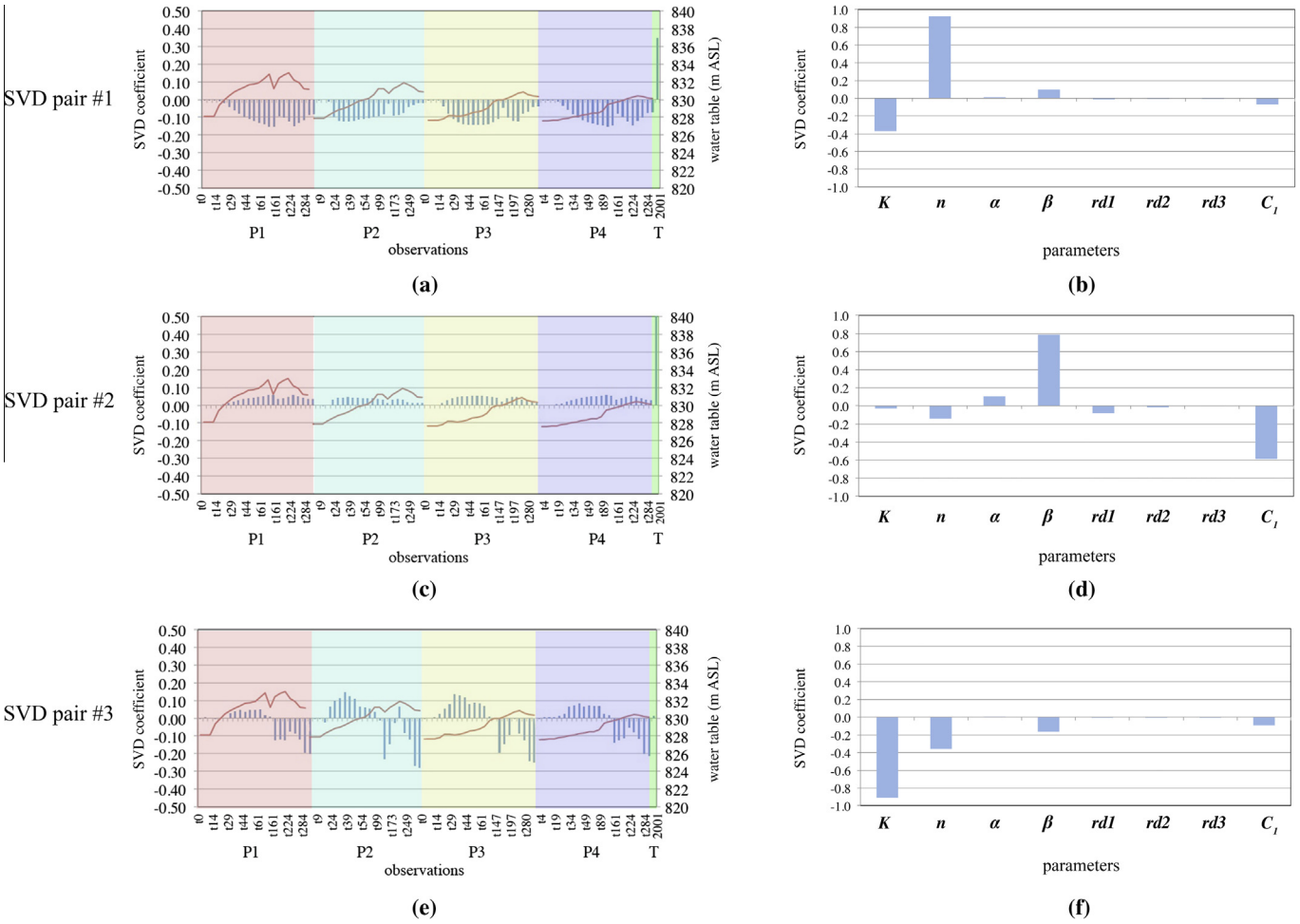

Fig. 10. Eigenvector pairs of the SVD analysis. On the left hand side, Eigenvectors of observations are illustrated. The horizontal axis shows all the groundwater head observations of the four wells that were used in the calibration (P1–P4), ordered by time and grouped by well, as well as the single transpiration observation (T). The primary vertical axis indicates the importance of each observation in informing the paired Eigenvector of parameters; a high absolute SVD coefficient represents high information content. The red line associated with the secondary vertical axis represents the elevation of the simulated groundwater table in each observation well. The Eigenvectors of parameters are shown in the right column of this figure. Every row represents an Eigenvector pair, each pair being associated with one Singular Value. The three pairs are ordered by the magnitude of their Singular Value, with the highest Singular Value and therefore the most important pair in top row.

Recall that observations with high, absolute SVD coefficients in the Eigenvectors of observations have high information content; they inform the parameters that have high, absolute SVD coefficients in the associated Eigenvectors of parameters. As already shown in Section 3.2 on data worth, plots 10a and 10c indicate high coefficients for transpiration and further support the finding that the information content of transpiration is high. The associated plots of Eigenvectors of parameters show that transpiration informs the inverse relation between the hydraulic conductivity (K) and the porosity (n) (represented by high coefficients in opposing directions in Fig. 10b) and to a lesser extent the relationship between the vegetation fitting parameter C_1 and the Van Genuchten parameter β (represented by high coefficients in opposing directions in Fig. 10d). Additionally, plot 10b shows that the relation between K and n is also informed considerably by observations of hydraulic head. This can be intuitively understood, as the relation between K and n is linked to the diffusivity of an aquifer, and this determines the speed of lateral propagation of groundwater movement. In the present case, this determines the time over which the water level is high, and over which water is thus available for transpiration by phreatic vegetation. Plots 10c and 10d also illustrate the high information content of transpiration data with respect to the unsaturated zone, represented by the high coefficients for both T and the parameter β. This might reflect the fact that water must undergo capillary rise through the unsaturated zone to replenish transpiration demands, as the relation between suction pressure and saturation is a function containing β in the exponent.

The combination of observations in plot 10e informs a similar combination of parameters as the combination of observations of plot 10a. The difference between the first (10a) and the third (10f) Eigenvector of parameters lies mainly in the algebraic signs of the SVD coefficients of the important parameters. Information in the third Eigenvector of observations (10e) lies in the interplay between the rise and fall of the groundwater levels, rather than in the interplay between groundwater levels and transpiration, as is the case for the first Eigenvector of observations (10a). This interplay is represented by the change from positive to negative coefficients for each piezometer after the first release.

4. Discussion

This study was motivated by an important environmental problem in western China, where *P. euphratica* forests along the lower Tarim River are endangered due to a dramatically reduced amount of available surface water. The ecological water releases initiated by the Chinese government, which started in 2000, aim at saving these forests. The efficiency of such measures has to be ensured.

Ecologists can provide estimates of the amount of water that is needed by the trees. However, numerical modeling is essential to quantify the amount of stream flow that is required to replenish the alluvial aquifers, which provide that water to the trees. The high number of parameters that have to be calibrated in such a numerical model simulating surface water, groundwater, and vegetation dynamics is in strong contrast to the limited amount of available observation data. We have explored an approach that allows significantly reducing the lack of data by using the historic information encapsulated in tree rings. In this paper we have demonstrated how such unconventional data can be included in the calibration dataset, we highlighted which parameters they inform, and we estimated the value of these data by quantifying how much these data reduce uncertainty of key predictions as a function of their measurement uncertainty. The specific implications of these analyses for the Tarim River site provide a solid basis for future data acquisition and modeling approaches targeting the optimization of the riparian water use efficiency.

While previous modeling attempts along the Tarim River focused solely on the information contained in groundwater level measurements (Yang et al., 2004), our predictive uncertainty analysis suggests that their use alone leaves an information deficit regarding transpiration and infiltration rates. We demonstrated that these deficits are related to the inability of such data to constrain the water balance (as shown in other studies, e.g. Brunner et al. (2012) and Doble et al. (2006)). This provides further evidence that measuring transpiration, and including these data into the modeling framework, is of outstanding importance for the quantification of surface water, groundwater, and vegetation dynamics.

In a novel attempt unique to this study, a relationship between depth to groundwater, tree ring growth, and transpiration was established and integrated in the calibration data set. The flow of information analysis showed that these indirect estimates of transpiration inform parameters required for the simulation of riparian dynamics. Specifically, the observations of transpiration inform parameters describing the unsaturated zone as well as parameters describing evapotranspiration processes. Counter-intuitively, even highly uncertain estimations of transpiration can improve the predictive performance of the model. In the absence of transpiration data parameters estimated on the basis of shallow groundwater measurements only are non-unique. As a consequence, the high predictive uncertainty of the simulations makes the optimization of ecological water releases very unreliable.

Our analyses for the Tarim River showed that tree ring growth data provide a possible proxy for transpiration. The current estimation of transpiration through tree ring growth should be improved, however, and complemented with more accurate, additional information, e.g. more tree ring samples as well as direct sap flow measurements during future flow releases. This information would allow using the historic data encapsulated in tree rings to their full potential, thus further increasing the predictive performance of the model. Finally, direct observations of infiltration should be measured as well, as this would allow constraining the water balance further.

Our simulations indicated that the riparian water use efficiency increased over time with increasing release event number. This is not a surprising result, as the water volume required to infiltrate and bring the water table within range of the root zone was reduced for each subsequent release due to locally retained recharge. Modeling has allowed this effect to be quantified. Such quantification is a vital input to the design of a long-term release strategy, in which, among other things, the relative effectiveness of large occasional releases will be balanced against those of smaller, more frequent releases. Other considerations will of course also play a part in such a design, including the timing of demand for irrigation by upstream users. This will lead to an optimization problem, in which modeling, supported by targeted data acquisition, should play a central role.

5. Conclusions

Integrated water resources management requires a quantitative understanding of the interactions and feedback mechanisms between groundwater, surface water, and vegetation processes. The Tarim River is a good example where such a holistic understanding of the system is essential for the successful restoration of the riparian vegetation. A complex numerical model capable of simulating riparian systems is required to respond to the pertinent questions of efficiency and sustainability of the different management options. A bottleneck to the application of such complex models is the lack of observation data. In fact, many hydrological or hydrogeological models are based solely on "classical" observations such as hydraulic heads or surface water runoff. These types of data, however, are insufficient to inform complex ecohydrological models, such as the Tarim model.

In this paper we demonstrated the importance of including transpiration estimates in the calibration data sets for models simulating riparian ecosystems. The inverse methods employed in our study allowed quantifying to what extent new observations reduce predictive uncertainties. Even though the uncertainties in estimating transpiration from tree rings are considerable for this specific field site, we could nonetheless show that the historic information encapsulated in tree rings is of substantial value. The wider ecohydrological community will benefit from exploring the largely untapped resources of information stored in tree rings to estimate historic transpiration. The inverse approaches applied in this context can easily be employed to other modeling applications. They can be used to explore the potential of any other type of observation data, providing a solid basis for efficient and targeted field data acquisition.

Acknowlegements

Philip Brunner was funded by the Swiss National Foundation, Ambizione grant PZ00P2_126415. John Doherty is funded by the National Centre for Groundwater Research and Training, Flinders University, GPO Box 2100, Adelaide, SA 5001, Australia. We also thank Li X. (Xinjiang Agricultural University, College of Agricultural and Environmental Science; Urumqi 830052) for the data on tree ring growth. We thank the editor Geoff Syme, Rebecca Doble, and the anonymous reviewers for their constructive comments and suggestions.

Appendix A. The mathematics of HydroGeoSphere

The following version of the Richards Eq. (1) for subsurface flow is used in HGS:

$$-\nabla \cdot (w_m q) + \sum \Gamma_{ex} \pm Q = w_m \frac{\partial}{\partial t}(\theta_s S_w) \quad (1)$$

S_w: degree of saturation [–].
Γ_{ex}: volumetric fluid exchange rate between the surface and the subsurface zone [$L^3\,L^{-3}\,T^{-1}$].
θ_S: saturated water content [–].
w_m: volumetric fraction of the total porosity occupied by the porous medium [–].
Q: fluid exchange with the outside of the simulation domain [$L^3\,L^{-3}\,T^{-1}$].

As we only simulate one porous medium and do not consider fractures, w_m is equal to 1. The fluid flux q [$L\,T^{-1}$] is outlined in Eq. (2) and contains the relative permeability $k_r = k_r(S_w)$ [–]:

$$q = -K \cdot k_r \nabla(\psi + z) \tag{2}$$

K: saturated hydraulic conductivity tensor [L T^{-1}].
ψ: pressure head [L].
z: elevation head [L].

Flow coupling between the surface zone and the subsurface porous medium is calculated with the dual node approach, where exchange is defined by Eq. (3):

$$d_0 \Gamma_0 = \frac{k_r K_{zz}}{l_{exch}} (H - H_0) \tag{3}$$

K_{zz}: vertical saturated hydraulic conductivity [L T^{-1}].
l_{exch}: coupling length [L].
H_0: surface water head [L].
H: subsurface water head [L].

The subsurface porous medium Eq. (4) relates the degree of saturation S_w to the pressure head ψ and Eq. (5) puts it in relation to the relative permeability k_r.

$$\begin{aligned} S_w &= S_{wr} + (1 - S_{wr})[1 + |\alpha\psi|^{\beta}]^{-\upsilon} \quad \text{for } \psi < 0 \\ S_w &= 1 \qquad\qquad\qquad\qquad\qquad\quad \text{for } \psi \geqslant 0 \end{aligned} \tag{4}$$

$$k_r(\psi) = S_e^{(l_p)} [1 - (1 - S_e^{1/\upsilon})^{\upsilon}]^2 \tag{5}$$

$$S_e = (S_w - S_{wr})/(1 - S_{wr}) \tag{6}$$

S_{wr}: residual water saturation [–].
α: Van Genuchten parameter [L^{-1}].
β: Van Genuchten parameter [–].
υ: given as $1–1/\beta$ with $\beta > 1$.
S_e: effective saturation [–].
l_p: pore-connectivity parameter (=2)

Li et al. (2008) describe the equations for the calculation of evapotranspiration (ET) used in HGS as follows: The potential evapotranspiration E_p represents the maximum possible amount of water than can be evaporated with unlimited water supply. Due to the negligible amount of rain, interception and thus canopy evaporation E_{canopy} becomes zero for the water balance in this study. Transpiration from vegetation in contrast, is very important. Key variables of the calculation of transpiration (7) are the leaf area index *LAI* [–] (8), the soil moisture content θ [–] (9), and the root distribution function *RDF* [–]. The *RDF* describes how with increasing depth fewer roots are present. In this study the *RDF* is a simple quadratic decay function.

$$T_p = f_1(LAI)\, f_2(\theta)\, RDF\, [E_p - E_{canopy}] \tag{7}$$

$$f_1(LAI) = \max\{0, \min[1, (C_2 + C_1 LAI)]\} \tag{8}$$

C_1, C_2: transpiration fitting parameters [–].

The function of soil water content $f_2(\theta)$ is a dependence term. Below the wilting point θ_{wp} [–] transpiration is zero. A maximum of transpiration is reached between the field capacity θ_{fc} [–] and the oxic limit θ_{ox} [–].

$$f_2(\theta) = \begin{cases} 0 & 0 \leqslant \theta \leqslant \theta_{wp} \\ f_3 & \theta_{wp} \leqslant \theta \leqslant \theta_{fc} \\ 1 \quad \text{for} & \theta_{fc} \leqslant \theta \leqslant \theta_{ox} \\ f_4 & \theta_{ox} \leqslant \theta \leqslant \theta_{an} \\ 0 & \theta_{an} \leqslant \theta \end{cases} \tag{9}$$

$$f_3 = 1 - \left[\frac{\theta_{fc} - \theta}{\theta_{fc} - \theta_{wp}}\right]^{C_3} \tag{10}$$

$$f_4 = 1 - \left[\frac{\theta_{an} - \theta}{\theta_{an} - \theta_{ox}}\right]^{C_3} \tag{11}$$

C_3: transpiration fitting parameter [–].
θ_{wp}: moisture content at wilting point [–].
θ_{fc}: moisture content at field capacity [–].
θ_{ox}: moisture content at oxic limit [–].
θ_{an}: moisture content at anoxic limit [–].

For further details on the mathematics of HGS consult the manual (Therrien et al., 2010).

References

Aster, R.C., Borchers, B., Thurber, C.H., 2005. Parameter estimation and inverse problems. In: International Geophysics 90. Academic Press, 296 pp..

Banks, E.W., Brunner, P., Simmons, C.T., 2011. Vegetation controls on variably saturated processes between surface water and groundwater and their impact on the state of connection. Water Resour Res 47.

Breda, N., Granier, A., 1996. Intra- and interannual variations of transpiration, leaf area index and radial growth of a sessile oak stand (*Quercus petraea*). Ann. Sci. For. 53, 521–536.

Brunner, P., Li, H.T., Kinzelbach, W., Li, W.P., Dong, X.G., 2008. Extracting phreatic evaporation from remotely sensed maps of evapotranspiration. Water Resour Res 8.

Brunner, P., Simmons, C.T., Cook, P.G., Therrien, R., 2010. Modeling surface water-groundwater interaction with MODFLOW: some considerations. Ground Water 48 (2), 174–180.

Brunner, P., Doherty, J.E., Simmons, C.T., 2012. Uncertainty assessment and implications for data acquisition in support of integrated hydrologic models. Water Resour Res 48.

Carsel, R.F., Parrish, R.S., 1988. Developing joint probability-distributions of soil-water retention characteristics. Water Resour. Res. 24 (5), 755–769.

Chen, Y.N. et al., 2008. Response of riparian vegetation to water-table changes in the lower reaches of Tarim River, Xinjiang Uygur, China. Hydrogeol. J. 16 (7), 1371–1379.

Chen, Y.N. et al., 2009. Effects of ecological water conveyance on groundwater dynamics and riparian vegetation in the lower reaches of Tarim River, China. Hydrol. Process 24 (2), 170–177.

Chen, Y.P., Chen, Y.N., Xu, C.C., Li, W.H., 2011. Groundwater depths affects the daily course of gas exchange parameters of Populus euphratica in arid areas. Environmental Earth Sciences (66), 433–440.

Christensen, S., Doherty, J.E., 2008. Predictive error dependencies when using pilot points and singular value decomposition in groundwater model calibration. Adv. Water Resour. 31 (4), 674–700.

Cui, Y.L., Shao, J.L., 2005. The role of ground water in arid/semiarid ecosystems, Northwest China. Ground Water 43 (4), 471–477.

Dausman, A.M., Doherty, J.E., Langevin, C.D., Sukop, M.C., 2010. Quantifying data worth toward reducing predictive uncertainty. Ground Water 48 (5), 729–740.

Doble, R., Simmons, C., Jolly, I., Walker, G., 2006. Spatial relationships between vegetation cover and irrigation-induced groundwater discharge on a semi-arid floodplain, Australia. J Hydrol (329), 75–97.

Doble, R., Brunner, P., McCallum, J., Cook, P.G., 2011. An analysis of river bank slope and unsaturated flow effects on bank storage. Ground Water 50 (1), 77–86.

Doherty, J.E., 2010a. PEST. Model-independent parameter estimation-User Manual (5th edition, with slight additions). Brisbane, Australia.

Doherty, J.E., 2010b. Addendum to the PEST Manual. Brisbane, Australia.

Doherty, J.E., Hunt, R.J., 2009. Two statistics for evaluating parameter identifiability and error reduction. J. Hydrol. 366 (1–4).

Doherty, J.E., Welter, D., 2010. A short exploration of structural noise. Water Resour Res 46 (5), 16.

Fu, A.H., Li, W.H., Chen, Y.N., Zhu, C.G., Ma, J.X., 2011. Analysis of dominant factors influencing moisture change of broad ovate-leaves of Populus euphratica Oliv. in extremely arid region. Photosynthetica 49 (2), 295–308.

GoogleEarth, 2003. Yingsu, Xinjiang, Western China. 40°26′2.75″N, 87°56′30.61″E. GoogleEarth 7.0.

Hill, M.C., Østerby, O., 2003. Determining extreme parameter correlation in ground water models. Ground Water 41 (4), 420–430.

Hill, M.C., Tiedemann, C.R., 2007. Effective Groundwater Model Calibration. John Wiley & Sons Inc., Hoboken, New Jersey, USA.

Hou, P., Beeton, R.J.S., Dong, X.G., Li, X., 2007. Response to environmental flows in the lower Tarim River, Xinjiang, China. J Environ Manage 83 (4), 371–382.

Hu, S.H., Zhao, R.F., Tian, C.Y., Song, Y.D., 2009. Empirical models of calculating phreatic evaporation from bare soil in Tarim river basin, Xinjiang. Environmental Earth Sciences 59 (3), 663–668.

Jarvis, A., Reuter, H.I., Nelson, A., Guevara, E., 2008. Hole-filled seamless SRTM data V4.

Kristensen, K.J., Jensen, S.E., 1975. A model for estimating actual evapotranspiration from potential evapotranspiration. Nord. Hydrol. 6 (3), 170–188.

Li, Q., Unger, A., Sudicky, E.A., Kassenaar, D., Wexler, E., Shikaze, S., 2008. Simulating the multi-seasonal response of a large-scale watershed with a 3D physically-based hydrologic model. J Hydrol 357 (3–4), 317–336.

Li, H.T., Brunner, P., Kinzelbach, W., Li, W.P., Dong, X.G., 2009. Calibration of a groundwater model using pattern information from remote sensing data. J. Hydrol. 377 (1), 120–130.

Ma, Z.G., Chen, X., Japper, G., Chang, C., 2009. Study on *LAI* estimation of broadleaf forests in arid areas using digital hemispherical photography – a case study in the Tarim River Basin, China. In: 2009 International Conference on Environmental Science and Information Technology, pp. 375–378.

Mitsch, W.J., Gosselink, J.G., 2007. Wetlands, fourth ed. John Wiley & Sons Inc., Hoboken, NJ, 582 pp.

Moriasi, D.N. et al., 2007. Model evaluation guidelines for systematic quantification of accuracy in watershed simulations. Trans. ASAE 50 (3), 885–900.

NASA, 2001. Taklamakan Desert, Western China, Visible Earth.

Panday, S., Huyakorn, P.S., 2004. A fully coupled physically-based spatially-distributed model for evaluating surface/subsurface flow. Adv. Water Resour. 27 (4), 361–382.

Si, J.H. et al., 2007. Sap flow of Populus euphratica in a desert riparian forest in an extreme arid region during the growing season. J. Integr. Plant Biol. 49 (4), 425–436.

Therrien, R., McLaren, R.G., Sudicky, E.A., 2010. HydroGeoSphere: A Three-dimensional Numerical Model Describing Fully-integrated Subsurface and Surface Flow and Solute Transport. Waterloo, Ontario, Canada.

Xu, H., Ye, M., Song, Y., Chen, Y., 2007. The natural vegetation responses to the groundwater change resulting from ecological water conveyances to the lower Tarim River. Environ. Monit. Assess. 131 (1–3), 37–48.

Yang, P.N., Li, X., 2011. Personal communication: tree ring growth records in Yingsu, Zurich/Urumqi.

Yang, P.N., Dong, X.G., Wumaierjiang, 2004. The simulation and analysis on a typical section of groundwater movement after transporting water to the lower reaches of Tarim River (in Chinese). J. Xinjiang Agric. Univ. 27 (3), 57–61.

Yu, P.J. et al., 2011. Effects of ecological water conveyance on the ring increments of Populus euphratica in the lower Tarim River. J For Res..